

Size control guidelines for chemically active droplets

Guido L. A. Kusters^{1,*} and David Zwicker¹

¹*Max Planck Institute for Dynamics and Self-Organization, Göttingen, Germany*

(Dated: December 3, 2025)

Biological cells and synthetic analogues use liquid-liquid phase separation to dynamically compartmentalize their environment for various applications. In many cases, multiple droplets need to coexist, and their size needs to be controlled, which is challenging because large droplets tend to grow at the expense of smaller ones. Chemical reactions can, in principle, control droplet sizes, but there are no clear guidelines on how to robustly achieve size control. To provide guidelines, we consider a binary fluid model driven out of equilibrium by chemical reactions. We reveal two different classes of size-controlled droplets, depending on the ratio of droplet radius to the reaction-diffusion length. Moreover, we determine parameter regimes in which droplets become small. Taken together, our theory allows us to separately predict the chemical reactions necessary for maintaining droplets of a given class or size.

I. INTRODUCTION

Many biological and synthetic systems rely on liquid-liquid phase separation for spatial organization. In particular, biological cells create liquid-like compartments that can regulate chemical reactions [1–5], buffer protein concentrations [6–9], and respond to external stresses [10–12]. In a similar vein, synthetic systems have been engineered to form hierarchical multiphase structures [13–16], create micro-reactors that concentrate enzymes or catalysts [17–21], program droplet (dis)assembly [22, 23], and sense environmental changes [24, 25]. In many of these applications, droplet size needs to be controlled, which remains a central design challenge.

One approach to regulating droplet size is through the use of chemical reactions. In the absence of reactions, droplets generally coarsen via Ostwald ripening [26–29], where large droplets grow at the expense of smaller ones and the system converges to a single minority-phase droplet at equilibrium. The size of such a droplet is dictated by the coexisting concentrations and the total amount of material, implying it cannot be tuned independently. Driven chemical reactions, however, can arrest or even reverse coarsening to enable size control. To describe this coupling, many initial works used linear rate equations [30–32], but more recent works have started to incorporate reaction schemes that explicitly obey the underlying thermodynamic constraints [33–35]. Although recent experimental advances indicate that such control can indeed be achieved [36–38], clear design guidelines for realizing stable, size-controlled droplets remain elusive.

In this paper, we address the question of droplet size control using a binary fluid model that is driven out of equilibrium by chemical reactions. The qualitative behavior of such a droplet is determined by its size as compared to the reaction-diffusion length—the typical distance a particle diffuses before undergoing a reaction—which introduces distinct classes of “small” and “large”

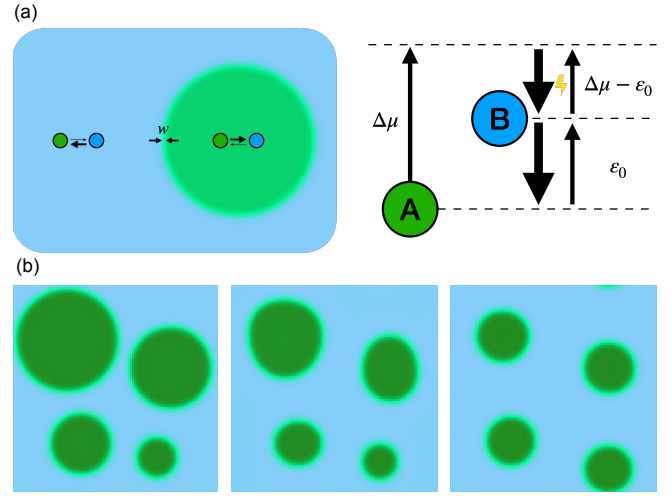


FIG. 1. **Conceptual model.** (a) Schematic representation of the model, in which components A and B segregate from each other and inter-convert through chemical reactions. The internal energy difference between the components, ϵ_0 , drives a passive reaction, while an active reaction is facilitated by an additional input of external energy, $\Delta\mu$. Concentration-dependent reaction rates can lead to differential production in the two phases. (b) Concentration field $\phi(\vec{r})$ at three time points illustrating effective droplet size control. Simulations of Eqs. (1)–(3) were done on a two-dimensional periodic grid of size $100w \times 100w$ and resolution $0.5w$ using `py-pde` [39] for model parameters $f(\phi) = \frac{B}{2}\phi^2(1-\phi)^2 - 0.05B\phi$, $\Delta\mu = 0.1B\nu$, $\Lambda_p(\phi) = 0.07[1 - \tanh(\frac{\phi-0.5}{0.01})]M$, $\Lambda_a(\phi) = 0.09[1 + \tanh(\frac{\phi-0.5}{0.01})]M$.

droplets. Alternatively, one may approach size control from the perspective of geometric constraints, and classify droplets as small or large compared to the length scale imposed by such constraints. Here, we show that the above views of droplet size control are not in general compatible, and we provide design guidelines for both.

* guido.kusters@ds.mpg.de

II. CONTINUUM MODEL OF CHEMICALLY ACTIVE DROPLETS

We consider an incompressible fluid comprising two components A and B that phase separate from each other. The volume fraction field $\varphi(\vec{r}, t)$ of component A fully describes the system since the fraction of B is $1 - \varphi$. The dynamical behavior of the fluid follows the continuity equation

$$\frac{\partial \varphi}{\partial t} + \vec{\nabla} \cdot \vec{J} = s, \quad (1)$$

where \vec{J} is a spatial flux and the source term s accounts for the conversion between A and B. For the model to be thermodynamically consistent, both fluxes must be driven by the exchange chemical potential

$$\mu = \nu \frac{\delta}{\delta \varphi} \int \left[f(\varphi) + \frac{\kappa}{2} |\nabla \varphi|^2 \right] dV, \quad (2)$$

where ν denotes a molecular volume scale, $f(\varphi)$ the free energy density, and κ a square-gradient coefficient that penalizes spatial gradients in composition [40].

Without reactions ($s = 0$), a suitable choice of $f(\varphi)$ leads to phase separation (Fig. 1). The equilibrium state is then characterized by the formation of “enriched” droplets, suspended in a “depleted” phase. In the thermodynamic limit, these phases have well-defined equilibrium compositions $\varphi_{\text{in}}^{(0)}$ and $\varphi_{\text{out}}^{(0)}$, respectively, and are separated by an interface with surface tension σ and width $w = \sqrt{\kappa/B}$, where B is the characteristic energy-density scale of $f(\varphi)$. In this passive system, surface tension drives coarsening [29], which implies that equilibria contain at most a single droplet. In finite systems, this droplet is spherical, characterized by a radius R . The coexisting compositions associated with this finite system are slightly elevated due to the surface tension effects, $\varphi_{\text{in}}^{\text{eq}} \approx \varphi_{\text{in}}^{(0)}$ and $\varphi_{\text{out}}^{\text{eq}} \approx \varphi_{\text{out}}^{(0)} [1 + 2\sigma\nu/(R\varphi_{\text{in}}^{(0)} k_B T)]$, where $k_B T$ denotes the thermal energy [32, 34, 41]. The physics of droplet formation is thus well-understood in passive systems, but activity modifies the picture.

To study the kinetics of active systems, we focus on linear non-equilibrium thermodynamics, where the spatial flux $\vec{J} = -M(\varphi)\vec{\nabla}\mu$ is driven by gradients in μ proportional to the diffusive mobility $M(\varphi)$ [42, 43]. In contrast, the reaction flux s is directly driven by μ ,

$$s = -\Lambda_p(\varphi)\mu - \Lambda_a(\varphi)(\mu + \Delta\mu). \quad (3)$$

The two terms in Eq. (3) respectively describe a *passive* reaction, whose conversion rate is proportional to μ , and an *active* reaction driven by an additional external energy input $\Delta\mu$ (Fig. 1(a)). The associated fluxes are proportional to the respective reaction mobilities Λ_p and Λ_a , which can depend on composition φ . For instance, biological reactions are often accelerated by enzymes, which might accumulate in the droplet. Taken together, Eqs. (1)-(3) can arrest or even reverse Ostwald ripening and give rise to droplet size control (Fig. 1(b)), in contrast to an equilibrium system.

III. THIN-INTERFACE APPROXIMATION

To analyze the dynamics of chemically active droplets in detail, we assume that reactions are weak, such that equilibrium phase coexistence holds approximately. More precisely, we assume that reactions do not significantly affect surface tension, interface width, and coexisting compositions at the droplet interface, so we can use the respective expressions for equilibrium interfaces. Droplets are then typically spherical, so we can parameterize them with their radius R . Assuming relatively large droplets ($R \gg w$), we then consider a thin interface and only account for reactions in the adjacent bulk regions. The dynamics of R are governed by the balance of diffusive fluxes at the interface,

$$\dot{R} = \frac{1}{\Delta\varphi} \left(-M_{\text{in}} \frac{\partial \mu_{\text{in}}}{\partial r} \Big|_R + M_{\text{out}} \frac{\partial \mu_{\text{out}}}{\partial r} \Big|_R \right), \quad (4)$$

where the subscripts refer to the droplet phase (“in”) and the surrounding dilute phase (“out”), respectively, and $\Delta\varphi = \varphi_{\text{in}}^{\text{eq}} - \varphi_{\text{out}}^{\text{eq}}$. Here, we have approximated the diffusive mobilities at either side of the thin interface, $M_{\text{in}} = M(\varphi_{\text{in}}^{(0)})$ and $M_{\text{out}} = M(\varphi_{\text{out}}^{(0)})$, by their values at the equilibrium compositions. The right-hand side of Eq. (4) depends on the chemical potential profiles $\mu_\alpha(\vec{r})$ in both phases. In the case of weak reactions, the variation of $\mu_\alpha(\vec{r})$ is limited, so we determine it by expanding Eq. (1) in the two phases $\alpha = \text{in}$ and $\alpha = \text{out}$,

$$\frac{\partial \varphi_\alpha}{\partial t} = M_\alpha \left(\nabla^2 \mu_\alpha - \frac{1}{l_{p,\alpha}^2} \mu_\alpha - \frac{1}{l_{a,\alpha}^2} (\mu_\alpha + \Delta\mu) \right), \quad (5)$$

where we assume that the aforementioned diffusive mobilities at either side of the thin interface, M_α , hold approximately throughout their respective phases. A similar approximation for reactive mobilities allows us to introduce reaction-diffusion lengths $l_{p,\alpha} = [M_\alpha/\Lambda_p(\varphi_\alpha^{(0)})]^{1/2}$ and $l_{a,\alpha} = [M_\alpha/\Lambda_a(\varphi_\alpha^{(0)})]^{1/2}$ for the passive and active reaction, respectively. Eq. (5) is subject to a no-flux condition at the system’s exterior boundary, which we take to be at infinity, implying sufficiently large systems. In contrast, equilibrium phase coexistence holds at the interface between the two phases, implying $\varphi_{\text{in}} = \varphi_{\text{in}}^{\text{eq}}$, $\varphi_{\text{out}} = \varphi_{\text{out}}^{\text{eq}}$, and $\mu_{\text{in}} = \mu_{\text{out}} = (-\varepsilon_0 + 2\sigma\nu R^{-1})/\Delta\varphi$ at the interface [32, 34, 41, 44], where $\varepsilon_0 = -\nu[f(\varphi_{\text{in}}^{\text{eq}}) - f(\varphi_{\text{out}}^{\text{eq}})]$ is the free energy difference per molecule between the two phases. The combination of Eqs. (4) and (5) fully determine the interface kinetics of an isolated active droplet.

To see when chemically active droplets are stable, we next solve Eq. (5) for the chemical potential profiles $\mu_\alpha(r)$, where r denotes the radial coordinate centered at the droplet center. Since the time scale on which the composition field φ relaxes is typically much faster than the time scale on which the droplet interface moves [44],

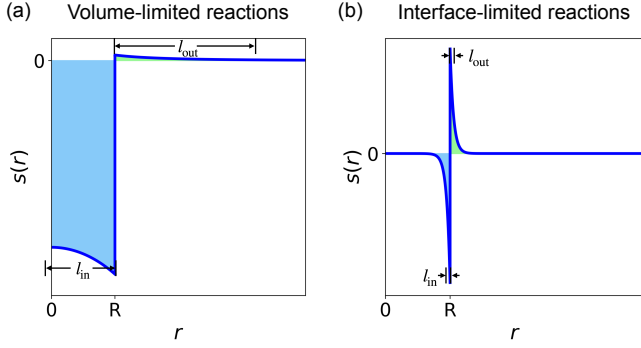


FIG. 2. **Volume-limited and interface-limited reactions.** Quasi-static reaction flux s as a function of the radial coordinate r for different values of l_{in} . The shaded blue and teal areas correspond to degradation and production of droplet material, respectively. (a) Model parameters are $\sigma = 0.15 Bw$, $\Delta\varphi = 1$, $\varepsilon_0 = 0.05 B\nu$, $\varepsilon_{\text{in}} = 0.05 B\nu$, $\varepsilon_{\text{out}} = -0.05 B\nu$, $l_{\text{in}} = 10^4 w$, $l_{\text{out}} = 1.11 \cdot 10^4 w$, and $R = 2 \cdot 10^5 w$. (b) Model parameters are $\sigma = 0.15 Bw$, $\Delta\varphi = 1$, $\varepsilon_0 = 0.01 B\nu$, $\varepsilon_{\text{in}} = 0.09 B\nu$, $\varepsilon_{\text{out}} = -0.01 B\nu$, $l_{\text{in}} = 500 w$, $l_{\text{out}} = 1000 w$, and $R = 455 w$.

we solve Eq. (5) in stationary state,

$$\mu_{\text{in}}(r) = \frac{\varepsilon_{\text{in}} + \frac{2\sigma\nu}{R}}{\Delta\varphi} \cdot \frac{\sinh\left(\frac{r}{l_{\text{in}}}\right)}{\sinh\left(\frac{R}{l_{\text{in}}}\right)} R - \frac{\varepsilon_{\text{in}} + \varepsilon_0}{\Delta\varphi}, \quad r \leq R, \quad (6a)$$

$$\mu_{\text{out}}(r) = \frac{\varepsilon_{\text{out}} + \frac{2\sigma\nu}{R}}{\Delta\varphi} \cdot \frac{e^{-\frac{r}{l_{\text{out}}}}}{e^{-\frac{R}{l_{\text{out}}}}} R - \frac{\varepsilon_{\text{out}} + \varepsilon_0}{\Delta\varphi}, \quad r > R, \quad (6b)$$

introducing the effective parameters

$$l_\alpha = \left(l_{a,\alpha}^{-2} + l_{p,\alpha}^{-2} \right)^{-\frac{1}{2}}, \quad \varepsilon_\alpha = \frac{\Delta\mu\Delta\varphi}{1 + l_{a,\alpha}^2 l_{p,\alpha}^{-2}} - \varepsilon_0, \quad (7)$$

for $\alpha = \text{in, out}$. To interpret these parameters, we substitute Eqs. (6) into Eq. (3) to obtain the local production of droplet material (Fig. 2). Looking at both phases separately, we find that the magnitude of the net turnover rate $|s|$ is greatest at the droplet interface, where its value is given by $s_\alpha = -M_\alpha(\varepsilon_\alpha + 2\sigma\nu R^{-1})/(l_\alpha^2 \Delta\varphi)$ in the respective phases, and decays further away from it. This identity suggests that ε_α contributes to the magnitude of the conversion rate and, perhaps more importantly, determines its sign, i.e., whether droplet material is locally produced ($s > 0$) or degraded ($s < 0$). Eqs. (6) show that the conversion rate falls off with characteristic length scales l_α away from the interface. This suggests chemical reactions inside the droplet may either occur throughout the entire droplet ($R \ll l_{\text{in}}$, Fig. 2(a)) or be concentrated at the interface ($R \gg l_{\text{in}}$, Fig. 2(b)).

To analyze the detailed dynamics of the droplet ra-

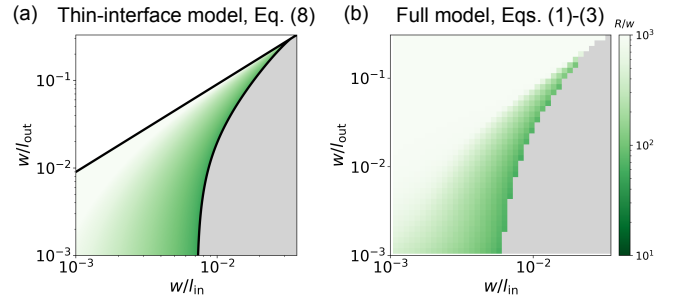


FIG. 3. **Thin-interface model captures stationary state radii.** Steady state droplet radius R as a function of the scaled reaction-diffusion lengths w/l_{in} and w/l_{out} . The system is homogeneously enriched in component A (white region), homogeneously enriched in component B (gray region), or exhibits an isolated droplet whose radius is indicated by color. (a) Data based on the stable fixed points of Eq. (8) for model parameters $\varepsilon_{\text{in}} = 0.09 B\nu$, $\varepsilon_{\text{out}} = -0.01 B\nu$, $\sigma = 0.15 B$, and $M_{\text{in}} = M_{\text{out}} = M$. (b) Data based on simulations of Eqs. (1)-(3) on a three-dimensional, spherically symmetric grid of radius $1000w$ and resolution $0.5w$ using `py-pde` [39] for the equivalent model parameters $f(\varphi) = \frac{B}{2}\varphi^2(1-\varphi)^2 - 0.01B\varphi$, $\Delta\mu = 0.1 B\nu$, $\Lambda_p(\varphi) = l_{\text{out}}^{-2}[1 - \tanh(\frac{\varphi-0.5}{0.01})]M$, $\Lambda_a(\varphi) = l_{\text{in}}^{-2}[1 + \tanh(\frac{\varphi-0.5}{0.01})]M$.

dius R , we insert Eqs. (6) into Eq. (4) to obtain

$$\dot{R} = -\frac{1}{R\Delta\varphi^2} \left[M_{\text{out}} \left(\varepsilon_{\text{out}} + \frac{2\sigma\nu}{R} \right) \left(1 + \frac{R}{l_{\text{out}}} \right) + M_{\text{in}} \left(\varepsilon_{\text{in}} + \frac{2\sigma\nu}{R} \right) \left(\frac{R}{l_{\text{in}}} \coth\left(\frac{R}{l_{\text{in}}}\right) - 1 \right) \right]. \quad (8)$$

The first term in the square brackets stems from the chemical reactions—and corresponding diffusive fluxes—outside the droplet, whereas the second term stems from reactions inside the droplet. The relative importance of these terms is governed by the diffusive mobilities M_α , the energy scales ε_α , and the reaction-diffusion lengths l_α . However, in the simple case without surface tension ($\sigma = 0$), only the product $M_\alpha \varepsilon_\alpha$ appears, indicating that these two parameters play similar roles. Since surface tension effects are typically small, we thus consider $M_{\text{in}} = M_{\text{out}}$ in what follows. Taken together, the key model parameters are ε_α and l_α , which influence the droplet radius R as the sole dynamical degree of freedom, governed by Eq. (8).

To check how well our approximate model captures the dynamics of the full system, we compare the stable fixed points of Eq. (8) with the final states observed from continuum simulations of Eq. (1). Fig. 3 shows that both methods agree very well, motivating us to use Eq. (8) as a predictive tool for understanding the behavior of chemically active droplets.

To see under which conditions droplets can be stable, we next analyze the steady states of Eq. (8) in detail. In the steady state, the reactions in the system balance globally, such that on average no net conversion between components persists. Since the signs of the energetic

prefactors $\varepsilon_\alpha + 2\sigma\nu/R$ dictate the direction of conversion (positive if droplet material is degraded and negative if it is produced), they must be opposite in the two regions to enable a non-trivial steady state. If we wish such a steady state to hold for arbitrarily large droplets ($2\sigma\nu/R \approx 0$), this leaves us with two distinct choices for ε_α : $\varepsilon_{\text{in}} > 0$, $\varepsilon_{\text{out}} < 0$ for *externally* maintained droplets (i.e., the droplet component A is produced outside the droplet and degraded inside the droplet) and $\varepsilon_{\text{in}} < 0$, $\varepsilon_{\text{out}} > 0$ for *internally* maintained droplets (i.e., the droplet component A is produced inside the droplet and degraded outside the droplet). A straightforward stability analysis reveals that only the former class admits *stable* steady-state solutions to Eq. (8) [32, 34, 45]. We thus focus on externally maintained droplets ($\varepsilon_{\text{in}} > 0$, $\varepsilon_{\text{out}} < 0$) in the rest of this paper.

IV. VOLUME- AND INTERFACE-LIMITED REACTIONS

We start by analyzing the qualitative behavior of externally maintained droplets. To this end, we single out the internal reaction-diffusion length l_{in} as the relevant length scale since it sets the distance over which the net conversion rate s extends into the droplet (Fig. 2). If $R \ll l_{\text{in}}$, the droplet is much smaller than the typical distance molecules diffuse before undergoing a chemical conversion (Fig. 2(a)). Consequently, we call such droplets “volume-limited”, as chemical conversions occur more or less homogeneously throughout the volume of the droplet. Conversely, if $R \gg l_{\text{in}}$, molecules that enter the droplet typically undergo a chemical conversion close to the interface, so we label such droplets “interface-limited” (Fig. 2(b)). The ratio R/l_{in} thus provides a natural interpretation of what it means for a droplet to be “small” or “large,” with distinct qualitative behavior for each.

We infer the behavior of volume- and interface-limited droplets by expanding Eq. (8) for $R/l_{\text{in}} \ll 1$ and $R/l_{\text{in}} \gg 1$, respectively, and solving for the stationary state. To build intuition, we first focus on droplets for which $R \gg 2\sigma\nu/\min(\varepsilon_{\text{in}}, |\varepsilon_{\text{out}}|)$, such that surface tension effects can be neglected. This is often a reasonable approximation if $R, l_{\text{in}} \gg w$, since the length scale $2\sigma\nu/\min(\varepsilon_{\text{in}}, |\varepsilon_{\text{out}}|)$ is in many typical cases comparable to the molecular length scale $\nu^{1/3}$ [32, 46]. In this limit, simple scaling

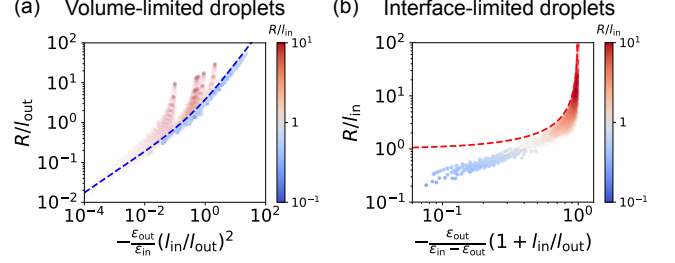


FIG. 4. **Volume-limited and interface-limited droplets obey scaling laws.** (a) Droplet radius R normalized by the external reaction-diffusion length l_{out} as a function of the control parameter expected for volume-limited droplets in comparison to the scaling law given by Eq. (9a) (dashed blue line). (b) R normalized to internal reaction-diffusion length l_{in} as a function of the control parameter expected for interface-limited droplets in comparison to the scaling law given by Eq. (9b) (dashed red line). (a, b) The colored data points represent stable fixed points of Eq. (8) for a range of parameter values. The color-coding is prescribed by the colorbar. Model parameters are $\sigma = 0.15 Bw$.

laws emerge:

$$\frac{R}{l_{\text{out}}} \approx -\frac{3}{2} \frac{\varepsilon_{\text{out}}}{\varepsilon_{\text{in}}} \left(\frac{l_{\text{in}}}{l_{\text{out}}} \right)^2 \left(1 + \sqrt{1 - \frac{4}{3} \frac{\varepsilon_{\text{in}}}{\varepsilon_{\text{out}}} \left(\frac{l_{\text{out}}}{l_{\text{in}}} \right)^2} \right), \quad R/l_{\text{in}} \ll 1, \quad (9a)$$

$$\frac{R}{l_{\text{in}}} \approx \frac{1}{1 + \frac{\varepsilon_{\text{out}}}{\varepsilon_{\text{in}} - \varepsilon_{\text{out}}} \left(1 + \frac{l_{\text{in}}}{l_{\text{out}}} \right)}, \quad R/l_{\text{in}} \gg 1, \quad (9b)$$

where $\varepsilon_{\text{in}} > 0$ and $\varepsilon_{\text{out}} < 0$ must hold for the stationary solutions to be stable. In either limit, the droplet radius R is governed by only two effective parameters, which suggests that the dependence on the four basic parameters (ε_{in} , ε_{out} , l_{in} , and l_{out}) can be drastically reduced. Indeed, numerically determined stationary state radii are well approximated by the scaling laws given by Eqs. (9) for volume-limited (blue data in Fig. 4(a)) and interface-limited (red data in Fig. 4(b)) droplets as a function of the reduced parameters.

To further probe under which conditions steady-state droplets of either regime can be expected, we investigate the stable fixed points of Eq. (8) in more detail. We first ask which combinations of the model parameters l_{in} , l_{out} , ε_{in} , and ε_{out} allow for steady-state droplets at all (Fig. 5). Our analysis reveals that, regardless of the values of ε_{in} and ε_{out} , stable droplets are precluded if either l_{in} is small and l_{out} is large, or l_{in} is large and l_{out} is small. This is because the reaction-diffusion lengths represent the relative importance of diffusion to reactions, with smaller values corresponding to faster reactions. As a result, the former case corresponds to a scenario in which the reactions produce droplet material much more

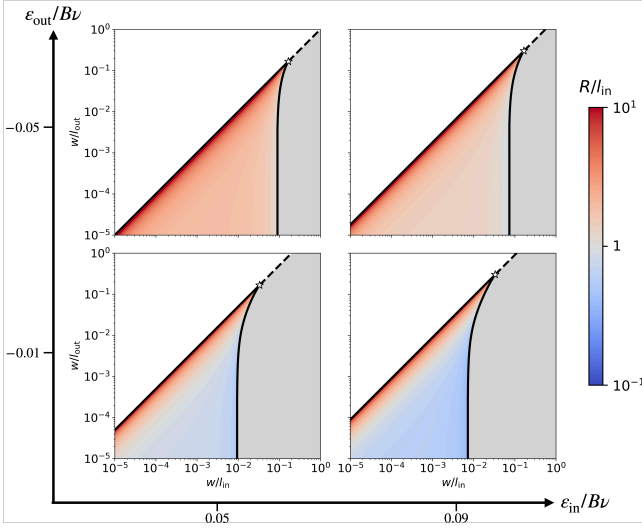


FIG. 5. **Parameter regions leading to volume- vs. interface-limited droplets.** Relative steady state droplet radius R/l_{in} as a function of the scaled reaction-diffusion lengths w/l_{in} and w/l_{out} . Each panel corresponds to a different combination of energy scales $\varepsilon_{\text{in}}/B\nu$ and $\varepsilon_{\text{out}}/B\nu$. The system is homogeneously enriched in component A (white region), homogeneously enriched in component B (gray region), or exhibits an isolated droplet whose radius is indicated by color. Model parameters are $\sigma = 0.15 Bw$.

quickly than they degrade it, such that the steady state becomes a homogeneous enriched phase (white regions in Fig. 5). The latter case corresponds to reactions that degrade droplet material much more quickly than they produce it, leading to a homogeneous depleted phase as the steady state (gray regions in Fig. 5). Consequently, steady-state droplets (colored region in Fig. 5) demand a balance between the reaction-diffusion length scales inside and outside of the droplet.

More concretely, the structure of the state diagram shown in Fig. 5 suggests that steady-state droplets can only exist if (i) their growth is halted at large droplet sizes (violated in the white region), and (ii) they overcome the inhibiting effect of surface tension (violated in the gray region). We quantify the region that admits steady-state droplets by determining when these conditions are met. Mathematically, the former condition demands that $\dot{R} < 0$ for large R . To locate the boundary beyond which condition (i) is violated, we thus take the limit of $R \rightarrow \infty$ in Eq. (8) and solve for $\dot{R} = 0$. Rearranging terms yields the asymptote

$$\frac{l_{\text{in}}}{l_{\text{out}}} = -\frac{\varepsilon_{\text{in}}}{\varepsilon_{\text{out}}}. \quad (10)$$

The second condition demands that $\dot{R} > 0$ for some range of R , since otherwise droplets of all sizes would shrink and eventually dissolve. Consequently, we find the boundary beyond which condition (ii) is violated by demanding that the growth rate \dot{R} peaks at $\dot{R} = 0$. The

parameter region where finite droplets are viable is enclosed by these two boundaries, which terminate at a critical point. The location of this critical point follows from expanding Eq. (8) for large R and setting the result to zero. The leading-order contribution reproduces Eq. (10), and the sub-leading-order contribution determines whether \dot{R} approaches its asymptotic value from above or below. Requiring that also this contribution vanishes gives

$$l_{\text{out},*} = \frac{2\sigma\nu}{\varepsilon_{\text{in}}}, \quad l_{\text{in},*} = -\frac{2\sigma\nu}{\varepsilon_{\text{out}}}; \quad (11)$$

see white star in Fig. 5. In particular, the critical point given by Eq. (11) helps us to limit the parameters for which droplet formation is possible.

To quantify admissible parameter regimes in more detail, we next measure the size of the region that exhibits stable droplets in steady state. As we vary ε_{in} and ε_{out} , the slope of the dashed asymptote and the location of the critical point shift, expanding or contracting this region. Taking the area under the asymptote given by Eq. (10) up to the critical point given by Eq. (11) as a rough estimate of this region's size, $-\frac{1}{8}\varepsilon_{\text{in}}\varepsilon_{\text{out}}w^2\sigma^{-2}\nu^{-2}$, we find that the product of energy scales $\varepsilon_{\text{in}}\varepsilon_{\text{out}}$ plays a key role in maximizing the number of reaction-rate combinations that lead to steady-state droplets. By symmetry of Eqs. (10) and (11), the same holds for the product $(l_{\text{in}}l_{\text{out}})^{-1}$ if one wishes to instead maximize the number of energy-scale combinations that yield steady-state droplets. We thus predict that increasing either $\varepsilon_{\text{in}}\varepsilon_{\text{out}}$ or $(l_{\text{in}}l_{\text{out}})^{-1}$ leads to more stable droplets. These trends are robust up to system-specific upper bounds for ε_{in} and $|\varepsilon_{\text{out}}|$, beyond which an instability can be triggered that leads to spinodal decomposition in the droplet phase or the dilute phase, respectively.

We next investigate how the model parameters can be tuned to access the regimes of volume- and interface-limited droplets, for which the ratio R/l_{in} is the determining factor. We find that increasing either the energy scale ($|\varepsilon_{\text{out}}|$) or rate ($1/l_{\text{out}}$) of the reaction that produces droplet material leads to an increase in R/l_{in} (blue to red in Fig. 5), as this biases the system to a steady state with a higher average volume fraction of droplet material. Conversely, increasing the energy scale (ε_{in}) or rate ($1/l_{\text{in}}$) of the reaction that degrades droplet material leads to a decrease in R/l_{in} (red to blue in Fig. 5). Amplifying the chemical reactions (through variation of ε_{α} and l_{α}) thus has opposite effects depending on whether they occur inside or outside the droplet.

To convert our observations into actionable design guidelines, recall that the effective parameters l_{α} and ε_{α} given by Eq. (7) depend on a variety of “bare” model parameters: the relevant active and passive reaction-diffusion lengths, $l_{a,\alpha}$ and $l_{p,\alpha}$, the internal energy difference ε_0 between components A and B, and the chemical drive $\Delta\mu$. Notably, our conclusions in terms of effective parameters do not translate one-to-one to these “bare” parameters, as both l_{α} and ε_{α} depend on $l_{a,\alpha}$ and $l_{p,\alpha}$. As

a result, variation of l_α does not, in general, keep ε_α constant. To nevertheless put our results into perspective, we consider the specific case where the chemical interconversion inside the droplet is dominated by an active reaction that degrades droplet material ($l_{\text{in}} = \sqrt{M/\Lambda_a}$, $\varepsilon_{\text{in}} = \Delta\mu\Delta\varphi - \varepsilon_0$), whereas the chemical interconversion outside the droplet is dominated by a passive reaction that produces droplet material ($l_{\text{out}} = \sqrt{M/\Lambda_p}$, $\varepsilon_{\text{out}} = -\varepsilon_0$). This introduces the passive reaction rate constant Λ_p , the internal energy difference ε_0 between components A and B, the active reaction rate constant Λ_a , and the chemical drive $\Delta\mu$ as independent and accessible control parameters. The former two are linked to the production of droplet material and increasing them promotes interface-limited droplets, whereas the latter two are linked to degradation and increasing them promotes volume-limited droplets. In addition, we showed above that the “area” of the droplet-forming region in Fig. 5 (i.e., the number of reaction-rate combinations ($l_{\text{in}}, l_{\text{out}}$) that admit steady-state droplets) scales with the product $|\varepsilon_{\text{in}}\varepsilon_{\text{out}}|$. If we substitute into this expression the parameters applicable to our specific case, it follows that the number of accessible reaction rate constant combinations (Λ_p, Λ_a) grows with increasing $\Delta\mu$ and reaches its maximum for $\varepsilon_0 = \frac{1}{2}\Delta\mu\Delta\varphi$. By symmetry, the number of admissible energy-scale combinations ($\varepsilon_{\text{in}}, \varepsilon_{\text{out}}$) scales with the product $l_{\text{in}}l_{\text{out}}$, which in our specific case translates to the number of admissible ($\varepsilon_0, \Delta\mu$) combinations scaling with the product of reaction rate constants $\Lambda_p\Lambda_a$.

Together, our findings show that the relative importance of external and internal parameters robustly determines whether volume- or interface-limited droplets form, regardless of the system specifications. The corresponding size scaling is well captured by Eqs. (9). In contrast, depending on the specific system, the likelihood of realizing a steady-state droplet in the first place is not necessarily improved by maximizing the available system parameters, but can exhibit intermediate optima.

V. DROPLET SIZE CONTROL

We next ask to what extent control over the qualitative behavior of droplets translates to droplet size control. In particular, we focus on how to realize small droplets, in order to accommodate the strict geometric constraints imposed by biological cells or synthetic applications. To do this, we investigate droplet size control by locating the stable fixed points of Eq. (8). Fig. 6 shows that boosting production of droplet material (increasing $1/l_{\text{out}}$, $|\varepsilon_{\text{out}}|$) increases droplet size (light shades of green), whereas boosting degradation (increasing $1/l_{\text{in}}$, ε_{in}) decreases droplet size (dark shades of green). This is qualitatively in line with our prior observations that the former promotes volume-limited droplets and the latter promotes interface-limited droplets. The beige region in Fig. 6(b) corresponds to the formation of unstable spherical shells through spinodal decomposition, which gener-

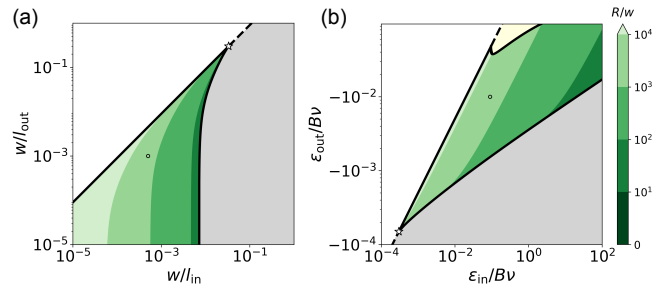


FIG. 6. **Parameter regions leading to small droplets.**

(a) Steady state radius R as a function of the two reaction-diffusion lengths, l_{in} and l_{out} , for $\varepsilon_{\text{in}} = 9 \cdot 10^{-2} B\nu$ and $\varepsilon_{\text{out}} = -10^{-2} B\nu$. (b) R as a function of the two energy scales, ε_{in} and ε_{out} , for $w/l_{\text{in}} = 5 \cdot 10^{-4}$ and $w/l_{\text{out}} = 10^{-3}$. (a, b) The system is homogeneously enriched in component A (white region), homogeneously enriched in component B (gray region), exhibits an isolated droplet whose radius is indicated by color, or exhibits complex dynamics due to an instability inside the droplet (beige region). Model parameters are $\sigma = 0.15 Bw$.

ally form if droplets are large [47].

The trends apparent from Fig. 6 suggest that the smallest droplets overall occur in a parameter regime that simultaneously minimizes $1/l_{\text{out}}$ and $|\varepsilon_{\text{out}}|$, and maximizes $1/l_{\text{in}}$ and ε_{in} . Note, however, that this is under the condition that a stable droplet forms in the first place, i.e., that production and degradation of droplet material balance globally. This constrains the admissible parameter values, as for a given combination of energy scales the reaction rates can only be made so fast before one dominates and destroys the stationary state; see the critical point given by Eq. (11). Concretely, this means that by maximizing the internal energy scale ε_{in} (boosting degradation), we make it possible for stable droplets to exist for increasingly high external reaction rates $1/l_{\text{out}}$ (boosting production). Consequently, it is possible to simultaneously maximize ε_{in} and minimize $1/l_{\text{out}}$. In contrast, if we minimize the external energy scale $|\varepsilon_{\text{out}}|$ (boosting production), this significantly limits how high the internal reaction rate $1/l_{\text{in}}$ (boosting degradation) can be. As a result, it is generally *not* possible to simultaneously minimize $|\varepsilon_{\text{out}}|$ and maximize $1/l_{\text{in}}$. To obtain the smallest droplets, a tradeoff must thus be made between the relative importance of the energy scale $|\varepsilon_{\text{out}}|$ and the reaction rate $1/l_{\text{in}}$.

To quantify under which conditions “small” droplets are most likely, we compute the corresponding range of admissible reaction-diffusion lengths $l_{\text{in/out}}$. To do this, we consider the area in Fig. 6(a) that corresponds to $R \leq 50w$, weighing each order of magnitude of $l_{\text{in/out}}$ equally. In essence, this corresponds to the probability of realizing a “small” droplet if one logarithmically samples all reaction-diffusion lengths plotted; the same qualitative behavior holds if we instead sample linearly. Fig. 7(a) shows that increasing either ε_{in} or $|\varepsilon_{\text{out}}|$ increases the likelihood of realizing “small” droplets. In

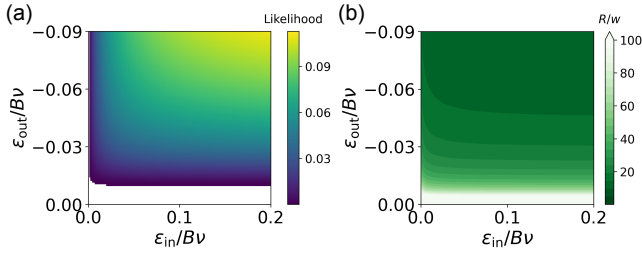


FIG. 7. **Parameter optimization for small droplet size.** (a) Likelihood of forming droplets for which $R \leq 50w$ in Fig. 6(a) as we vary $\epsilon_{in}/B\nu$ and $\epsilon_{out}/B\nu$. We weigh each order of magnitude equally and keep the scanning window constant: $w/l_{in} \in [10^{-5}, 1]$, $w/l_{out} \in [10^{-5}, 1]$. (b) Corresponding achievable minimum droplet size R/w . Model parameters are $\sigma = 0.15 Bw$.

a similar vein, Fig. 7(b) shows the smallest droplet size achievable for any given combination of energy scales, thus illustrating the range of possible droplet sizes. This figure shows that the smallest droplets are achieved by maximizing both ϵ_{in} and $|\epsilon_{out}|$. These results suggest that maximizing the internal reaction rate, related to $1/l_{in}$, weighs more heavily than minimizing the external energy scale, $|\epsilon_{out}|$, in the pursuit of small droplets.

Notably, Fig. 7 contrasts with our prior observations that simultaneously maximizing ϵ_{in} and minimizing $|\epsilon_{out}|$ promotes volume-limited droplets ($R/l_{in} \ll 1$). This is because for a droplet to be volume limited, its size must be small *relative* to the internal reaction-diffusion length l_{in} . As a result, although maximizing the internal reaction rate $1/l_{in}$ produces the smallest droplets overall, it also biases droplets toward the interface-limited regime by decreasing l_{in} . Our results indicate that this shifts the balance between $|\epsilon_{out}|$ and $1/l_{in}$: in the pursuit of volume-limited droplets, minimizing $|\epsilon_{out}|$ weighs more heavily than maximizing $1/l_{in}$ (Fig. 5).

Translated to the specific case discussed in the previous section—passive production of droplet material outside the droplet and active degradation inside—we propose the following design guidelines: Increasing the passive reaction rate constant Λ_p promotes large droplets, whereas increasing the active reaction rate constant Λ_a or the chemical drive $\Delta\mu$ promotes small droplets. This aligns with the design guidelines for obtaining volume-limited droplets. In contrast, while increasing ϵ_0 increases droplet size at fixed conditions, the smallest droplets overall occur at intermediate values of $0 < \epsilon_0 < \Delta\mu/\Delta\phi$, due to the accessible region of the phase diagram shrinking. This differs from the parameter regime for which the most strongly volume-limited droplets are expected, which occurs for minimal values of ϵ_0 . We thus conclude that if one keeps the energy scales of the chemical reactions constant, increasing the rate constant of the droplet-material-producing reaction promotes larger droplets, whereas increasing the rate constant of the droplet-material-degrading reaction promotes smaller droplets. Similarly, if one keeps the rate

constants constant, increasing the energy scale driving the droplet-material-producing reaction promotes larger droplets, whereas increasing the energy scale driving of the droplet-material-degrading reaction promotes smaller droplets. If we vary all parameters simultaneously, however, the smallest droplets are achieved by increasing both energy scales, because this choice enlarges the region of the state diagram that admits steady-state droplets. This indicates that the design guidelines for obtaining small droplets are different from those for obtaining volume-limited droplets, reinforcing the importance of their distinction.

VI. CONCLUSION AND DISCUSSION

We have studied droplet stability and size control within a binary fluid model driven out of equilibrium by chemical reactions. We have identified four key parameters that predict the steady state of such droplets in good agreement with continuum simulations: the effective reaction-diffusion lengths, l_{in} and l_{out} , and the effective energy scales, ϵ_{in} and ϵ_{out} . We show that if one takes l_{in} as the natural length scale for droplet size, unambiguous classes of volume-limited ($R/l_{in} \ll 1$) and interface-limited ($R/l_{in} \gg 1$) droplets arise, which obey simple scaling laws. By tuning the relative importance of the production ($l_{out}^{-1}, \epsilon_{out}$) and degradation ($l_{in}^{-1}, \epsilon_{in}$) of droplet material, we can transition between these regimes. Although this view of size control governs qualitative droplet behavior, it does not necessarily accommodate exact geometric constraints, as are present in biological cells and synthetic applications. Importantly, we show that the design guidelines for realizing small droplets deviate qualitatively from the design guidelines for realizing volume-limited droplets ($R/l_{in} \ll 1$).

Concretely, our findings indicate that in order to achieve “small” droplets, a tradeoff must be made between the energetics and the kinetics of the associated chemical reactions. This is because the reaction rates dictate the range of energy scales that admit steady-state droplets and *vice versa*, implying that it is not generally possible to optimize for both simultaneously. If we take “small” to mean volume limited, it turns out that we must prioritize the energetics, and our recommendation is to minimize l_{out}^{-1} , $|\epsilon_{out}|$ and maximize l_{in}^{-1} , ϵ_{in} . If we instead take “small” to refer to the absolute size of the droplet, we must prioritize the kinetics, resulting in the recommendation to minimize l_{out}^{-1} and maximize l_{in}^{-1} , ϵ_{in} , $|\epsilon_{out}|$. This tradeoff suggests that the qualitative behavior of the droplet and its absolute size could in principle be tuned separately. We speculate that this might allow cells and synthetic applications to further specialize condensates to fulfill specific functions, such as buffering or regulation [6–9, 48–50], even under geometric constraints.

More broadly, our work serves as a point of departure for understanding droplet size control in more general contexts. An obvious extension would be to study emul-

sions of closely interacting droplets [51, 52], rather than isolated droplets. Similarly, it would be interesting to study systems with more than two components [52, 53], which exhibit conserved quantities that can vary in space. In addition, droplets in many biological contexts contend with much more complex, elastic micro-environments, which are known to affect their dynamics [54–57]. Finally, we considered droplet size control in the deterministic limit, but how thermal fluctuations affect droplet size control remains an outstanding question; especially

considering that thermal energy should be relevant on the typical length and energy scales of many (biological) droplets.

Acknowledgments

We gratefully acknowledge funding from the Max Planck Society and the European Research Council (ERC, EmulSim, 101044662).

-
- [1] A. A. Hyman, C. A. Weber, and F. Jülicher, *Annu. Rev. Cell Dev. Biol.* **30**, 39 (2014).
 - [2] S. F. Banani, H. O. Lee, A. A. Hyman, and M. K. Rosen, *Nat. Rev. Mol. Cell Biol.* **18**, 285 (2017).
 - [3] S. Alberti, *J. Cell Sci.* **130**, 2789 (2017).
 - [4] J. Berry, C. P. Brangwynne, and M. Haataja, *Rep. Prog. Phys.* **81**, 046601 (2018).
 - [5] K. Lasker, S. Boeynaems, V. Lam, D. Scholl, E. Stainton, A. Briner, M. Jacquemyn, D. Daelemans, A. Deniz, E. Villa, *et al.*, *Nat. Commun.* **13**, 5643 (2022).
 - [6] A. Klosin, F. Oltsch, T. Harmon, A. Honigmann, F. Jülicher, A. A. Hyman, and C. Zechner, *Science* **367**, 464 (2020).
 - [7] D. Deviri and S. A. Safran, *Proc. Natl. Acad. Sci. U.S.A.* **118**, e2100099118 (2021).
 - [8] C. Zechner and F. Jülicher, *Cell Syst.* **16** (2025).
 - [9] L. de Monchaux-Irons, T. Y. Tang, C. A. Weber, and T. C. T. Michaels, *Dynamic principles of concentration buffering through liquid-liquid phase separation* (2025), 2510.20553 [physics].
 - [10] C. P. Brangwynne, C. R. Eckmann, D. S. Courson, A. Rybarska, C. Hoege, J. Gharakhani, F. Jülicher, and A. A. Hyman, *Science* **324**, 1729 (2009).
 - [11] J. R. Wheeler, T. Matheny, S. Jain, R. Abris, and R. Parker, *eLife* **5**, e18413 (2016).
 - [12] H. Yoo, J. A. Bard, E. V. Pilipenko, and D. A. Drummond, *Mol. Cell* **82**, 741 (2022).
 - [13] X. Ge, A. J. Conley, J. E. Brandle, R. Truant, and C. D. Filipe, *J. Am. Chem. Soc.* **131**, 9094 (2009).
 - [14] M. Dzuricky, B. A. Rogers, A. Shahid, P. S. Cremer, and A. Chilkoti, *Nat. Chem.* **12**, 814 (2020).
 - [15] D. T. Tomares, S. Whitlock, M. Mann, E. DiBernardo, and W. S. Childers, *ACS Synth. Biol.* **11**, 2154 (2022).
 - [16] J. Liao, V. Yeong, and A. C. Obermeyer, *ACS Synth. Biol.* **13**, 598 (2024).
 - [17] S. Koga, D. S. Williams, A. W. Perriman, and S. Mann, *Nat. Chem.* **3**, 720 (2011).
 - [18] B. Saha, A. Chatterjee, A. Reja, and D. Das, *Chem. Commun.* **55**, 14194 (2019).
 - [19] A. M. Küffner, M. Prodan, R. Zuccarini, U. Capasso Palmiero, L. Faltova, and P. Arosio, *ChemSystem-sChem* **2**, e2000001 (2020).
 - [20] W. Peeples and M. K. Rosen, *Nat. Chem. Biol.* **17**, 693 (2021).
 - [21] I. B. A. Smokers, B. S. Visser, A. D. Sloodbeek, W. T. S. Huck, and E. Spruijt, *Acc. Chem. Res.* **57**, 1885 (2024).
 - [22] J. Deng and A. Walther, *Chem* **6**, 3329 (2020).
 - [23] C. Donau and J. Boekhoven, *Trends Chem.* **5**, 45 (2023).
 - [24] K. Lv, A. W. Perriman, and S. Mann, *Chem. Commun.* **51**, 8600 (2015).
 - [25] E. Jambon-Puillet, A. Testa, C. Lorenz, R. W. Style, A. A. Rebane, and E. R. Dufresne, *Nat. Commun.* **15**, 3919 (2024).
 - [26] W. Ostwald, *Z. Phys. Chem.* **22**, 289 (1897).
 - [27] I. M. Lifshitz and V. V. Slyozov, *J. Phys. Chem. Solids* **19**, 35 (1961).
 - [28] C. Wagner, *Z. Elektrochem., Ber. Bunsenges. Phys. Chem.* **65**, 581 (1961).
 - [29] P. W. Voorhees, *J. Stat. Phys.* **38**, 231 (1985).
 - [30] D. Zwicker, A. A. Hyman, and F. Jülicher, *Phys. Rev. E* **92**, 012317 (2015).
 - [31] J. D. Wurtz and C. F. Lee, *Phys. Rev. Lett.* **120**, 078102 (2018).
 - [32] C. A. Weber, D. Zwicker, F. Jülicher, and C. F. Lee, *Rep. Prog. Phys.* **82**, 064601 (2019).
 - [33] J. Kirschbaum and D. Zwicker, *J. R. Soc. Interface* **18**, 20210255 (2021).
 - [34] D. Zwicker, O. Paulin, and C. Ter Burg, *Rep. Prog. Phys.* **88**, 116601 (2025).
 - [35] J. Bauermann, G. Bartolucci, C. A. Weber, and F. Jülicher, *Phys. Rev. Lett.* **135**, 148201 (2025).
 - [36] Y. Dai, L. You, and A. Chilkoti, *Nat. Rev. Bioeng.* **1**, 466 (2023).
 - [37] J. Sastre, A. Thatte, A. M. Bergmann, M. Stasi, M. Tena-Solsona, C. A. Weber, and J. Boekhoven, *Nat. Commun.* **16**, 2003 (2025).
 - [38] T. Ura, T. Yoshida, T. Mikawa, and K. Shiraki, *Polym. J.*, 1 (2025).
 - [39] D. Zwicker, *J. Open Source Softw.* **5**, 2158 (2020).
 - [40] J. W. Cahn, *Acta metallurgica* **9**, 795 (1961).
 - [41] W. Thomson, *Proc. R. Soc. Edinb.* **7**, 63 (1872).
 - [42] L. Onsager, *Phys. Rev.* **37**, 405 (1931).
 - [43] S. R. De Groot and P. Mazur, *Non-equilibrium thermodynamics* (Dover Publications, 1984).
 - [44] A. J. Bray, *Adv. Phys.* **43**, 357 (1994).
 - [45] D. Zwicker, *Curr. Opin. Colloid Interface Sci.* **61**, 101606 (2022).
 - [46] E. M. Lifshitz and L. P. Pitaevskii, *Physical Kinetics*, Vol. 10 (Butterworth-Heinemann, 2012).
 - [47] A. M. Bergmann, J. Bauermann, G. Bartolucci, C. Donau, M. Stasi, A.-L. Holtmannspötter, F. Jülicher, C. A. Weber, and J. Boekhoven, *Nat. Commun.* **14**, 6552 (2023).
 - [48] W. T. Snead and A. S. Gladfelter, *Mol. Cell* **76**, 295 (2019).

- [49] J. Söding, D. Zwicker, S. Sohrabi-Jahromi, M. Boehning, and J. Kirschbaum, *Trends Cell Biol.* **30**, 4 (2020).
- [50] S. Jeon, Y. Jeon, J.-Y. Lim, Y. Kim, B. Cha, and W. Kim, *Signal Transduct. Target. Ther.* **10**, 4 (2025).
- [51] S. Köstler, Y. Qiang, G. Kusters, and D. Zwicker, *Advection selects pattern in multi-stable emulsions of active droplets* (2025), 2510.00827 [cond-mat].
- [52] J. Bauermann, G. Bartolucci, J. Boekhoven, F. Jülicher, and C. A. Weber, *Phys. Rev. X* **15**, 041027 (2025).
- [53] Y. Qiang, C. Luo, and D. Zwicker, *Generic multicomponent mixtures are multistable* (2024), 2405.01138 [cond-mat].
- [54] E. Vidal-Henriquez and D. Zwicker, *Soft Matter* **16**, 5898 (2020).
- [55] E. Vidal-Henriquez and D. Zwicker, *Proc. Natl. Acad. Sci. U.S.A.* **118**, e2102014118 (2021).
- [56] O. Paulin, Y. Qiang, and D. Zwicker, *Dynamics of phase separation in non-local elastic networks* (2025), 2508.09829 [cond-mat].
- [57] P. Ronceray, S. Mao, A. Kosmrlj, and M. P. Haataja, *Eur. Lett.* **137**, 67001 (2022).